



# Machine Learning-aided Sensing in Private mmWave Networks for Industrial Applications

Marcus Haferkamp, Simon Häger, Stefan Böcker, and Christian Wietfeld

Communication Networks Institute (CNI), TU Dortmund University, 44227 Dortmund, Germany

E-mail: {Marcus.Haferkamp, Simon.Haeger, Stefan.Boecker, Christian.Wietfeld}@tu-dortmund.de

**Abstract**—Integrated sensing and communication (ISAC) is set to become crucial in future wireless networks as it enables enhanced communication performance while simultaneously providing ambient sensing services to verticals. This is expected to be particularly important in industrial environments, where real-time detection and classification are vital to improving automation efficiency and maintaining safety. This paper showcases the wireless channel of distributed connected devices as a privacy-preserving sensor characteristically affected by ambient mobility of automated guided vehicles (AGVs) and humans, thus enabling 6G edge intelligence-based sensing services. We propose the hybrid machine learning (ML) approach **Integrated ML-aided mmWave Radio Sensing (IMMERSE)**, combining data, context, and knowledge to realize passage detection, user classification, and movement direction estimation. We validate IMMERSE using real-world received power traces from our measurements with a non-standalone millimeter-wave (mmWave) network and feature extraction-enabled lightweight ML. For user detection and classification, we observe an accuracy of up to 100 %, which is superior to leveraging sub-6 GHz anchor band channel state information (CSI). By aggregating multiple radio links, we achieve a movement direction estimation with 97.7 % accuracy.

**Index Terms**—6G Integrated Sensing and Communications, Industrial Private Networks, Millimeter-wave, Edge Intelligence, User Classification, Machine Learning.

## I. INTRODUCTION

Upcoming 6G networks promise to revolutionize wireless networks by improving communication throughput and latency as well as seamless and synergistic integration within versatile application scenarios. The pivotal approaches identified by academia and industry are the integrated sensing and communication (ISAC) and edge intelligence (EI) paradigms, which enable novel use cases for verticals, such as traffic monitoring, pedestrian detection, and motion direction sensing [1]. In this work's context, 6G becomes the backbone of future digital economies by enabling industry automation by private network deployments.

By integrating sensing functionalities, ISAC changes how the operator employs mobile radio networks, particularly those operating at mmWave frequencies. For instance, ISAC can empower 6G systems to become perceptive networks with enhanced situational awareness, e.g., helping to improve the overall communication performance by improved beam management [2]. Moreover, the gained context information can be leveraged in automated industry facilities to track and orchestrate automated guided vehicles (AGVs). It additionally facilitates an autonomous and privacy-preserving detection of human workers, helping avoid dangerous collisions with AGVs.

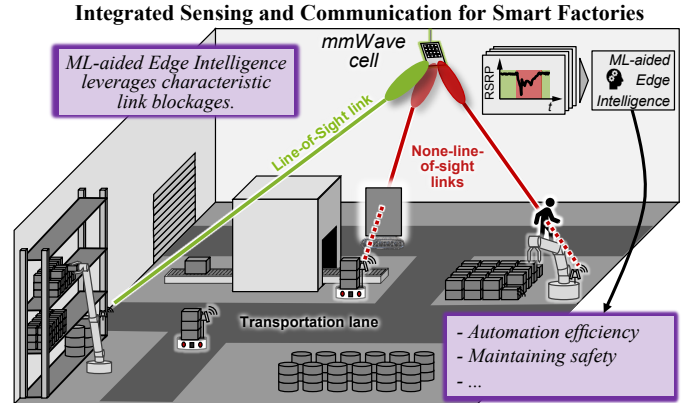


Fig. 1. Future 6G networks will be part of industrial value chains. For example, novel sensing features and edge intelligence enable factory automation.

Fig. 1 depicts these industrial use cases of 6G ISAC and the proposed solution approach. Following the radio fingerprinting principle of its dedicated predecessor system deployment for road traffic detection and classification [3], a base station (BS) continuously monitors channel state information (CSI) metrics of connected stationary and mobile users. Whenever AGVs or pedestrians traverse, they induce characteristic attenuation patterns to the radio channels, exploitable for safety-critical in-factory applications requiring detection and classification of different users. Moreover, by aggregating CSI of distributed user equipment (UE) links, the network can estimate the specific trajectory of the users, yielding a synergy of sensing and communication. In future industry network deployments, these tasks are expected to be performed by state-of-the-art ML techniques at the edge of the network.

Our key contributions are summarized as follows:

- We conduct extensive indoor measurements of a cellular mmWave system's CSI traces for various mobile users utilizing distributed commercial UEs. This work showcases the suitability of spatiotemporal received signal strength power (RSSP) traces for an ML-enabled industry shop floor automation.
- Our solution approach, Integrated ML-aided mmWave Radio Sensing (IMMERSE), implements an EI-centric process, incorporating efficient feature extraction and selection, and compares the classification performances of lightweight and modern ML models.
- We provide a sensing performance analysis for (i) user classification and (ii) passage direction estimation, comparing mmWave and anchor band CSI.

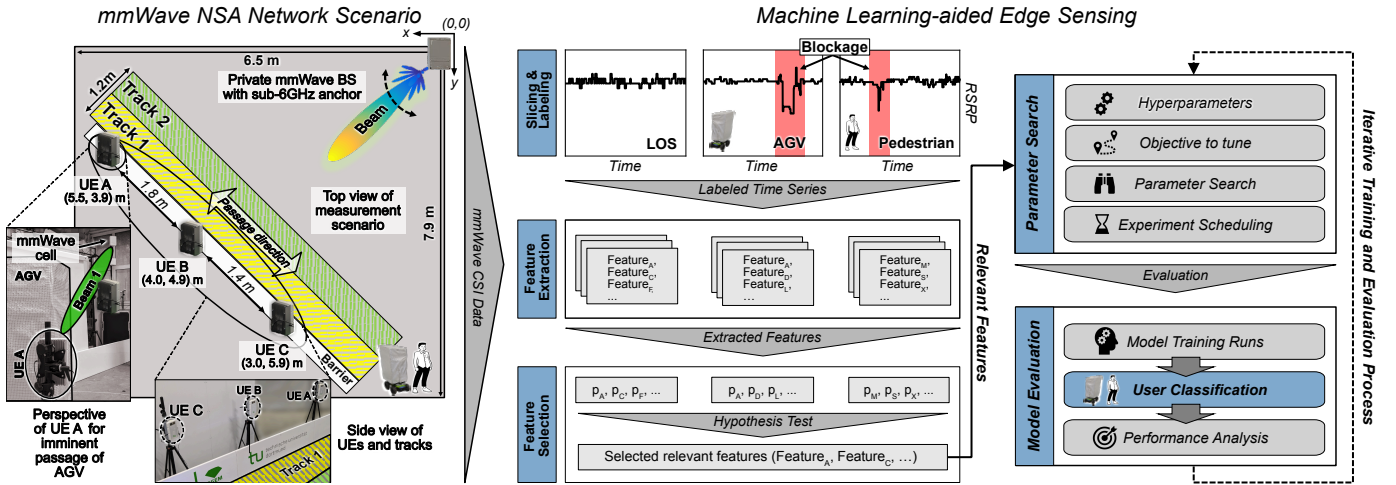


Fig. 2. Solution approach for 6G edge intelligence-based traffic sensing on shop floors using CSI from private mmWave radio access network (RAN).

- We release the CSI measurement data, fostering researchers to evaluate novel radio-based sensing methods for future 6G networks [17].

The rest of this manuscript is structured as follows. After discussing related work on 6G sensing in Sec. II, Sec. III describes our measurement methodology and the developed solution approach IMMERSE. We then evaluate the approach's performance for user classification and mobility direction estimation in Sec. IV. Last, Sec. V concludes with a summary of this work and a brief outlook on future work.

## II. RELATED WORKS

The addition of sensing services to 6G has been initiated by extended positioning service capabilities in 5G using power, time, and angle channel parameters [4]. Moving towards 6G, radar-like sensing is expected to provide high-quality data for various applications [5]. The ongoing Wi-Fi sensing standardization activities have set similar goals [6]. Both wireless approaches agree that mmWave carriers in the frequency range 2 (FR2) band are more suitable than sub-6GHz carriers (frequency range 1 (FR1)). Due to the available broad bandwidth and adopted beamforming antenna arrays, FR2 allows the realization of high spatiotemporal sensing resolution and reduced clutter.

The acquired sensing data allows for radio access technology (RAT)-internal or -external use helping to improve the communication performance, e.g., by proactively switching antenna beams to a reconfigurable intelligent surface (RIS)-aided non-line-of-sight (NLOS) path if the line-of-sight (LOS) path is obstructed. Among others, the sensing information enables a situation-aware increase of the transmit power, selecting robust modulation and coding schemes (MCSs) or initiating a handover. These measures reduce a system's communication overhead while optimizing performance [2, 7, 8].

In the second use case, the cellular network transforms into a perceptive environment sensor that may gather its environment, allowing it to localize mobile users (e.g., AGVs, humans) and even detect their gestures without needing them

to be connected. Whereas there is undoubtedly a high potential for radar-based sensing, seamless integration is a challenging multidisciplinary task for the coming years toward 6G. Moreover, recent research has investigated radio-native sensing approaches primarily based on different radio channel metrics. Advantages include, for example, reduced sensing overhead, less complexity and costs, and native privacy [3, 9]. Multiple promising studies leverage CSI time series for an ML-aided prediction of future mmWave link blockages to trigger RAT-internal performance optimization [2, 7, 10–12]. Otherwise, we have recently demonstrated that mmWave channel data, provided by the DeepSense dataset [2], is apt for being exploited for RAT-external services in the scope of future intelligent transportation systems (ITSs). Such sensing data may empower distributed road traffic monitoring, including counting and classifying different road users, e.g., humans and vehicles, and flow direction estimation [13].

Against this background, this work moves from a channel sounder-based approach with CSI available for all antenna beam configurations to a commercial mmWave-based cellular network deployment with multiple connected commercial off-the-shelf (COTS) UEs. Our motivation is to assess the potential of private cellular networks as wireless sensors for verticals. In this work, we assume an indoor industry shop floor scenario, facilitating factory automation and improving worker safety by monitoring human and machine mobility in a privacy-preserving manner without a dedicated system. Additional points of interest include comparing mmWave (serving cell) and sub-6GHz (anchor cell) sensing performances [14] and investigating multilink CSI-based user classification [15].

## III. MEASUREMENTS AND IMMERSE APPROACH

This section presents this work's methodology, including our hybrid ML solution approach, *Integrated ML-aided mmWave Radio Sensing* (IMMERSE), which combines real-world CSI data and environment knowledge for industrial sensing applications, cf. Fig. 2. First, Sec. III-A introduces the indoor environment and cellular network setup for gath-

TABLE I. MMWAVE NETWORK DEPLOYMENT SCENARIO DETAILS [16].

Parameter	Description/Value	
BS	mmWave Radio Unit	Ericsson AIR 1281
	Frequency Band	5G NR band n257 (26.7 GHz to 27.5 GHz)
	TDD Pattern	DDSU, 11:3:0
	Max. Transmit Power	20 dBm / 100 mW (EIRP)
	Anchor Cell	LTE band 7 (FDD) with 20 MHz bandwidth
UE	Device Model	Quectel 5GDM01EK + RG530F-EU
	Modem and Antennas	Qualcomm SDX65, RA530T + 4x QTM547
	Power Class	Class 3 (max. 23 dBm / 200 mW)
	Capabilities	2 × 2 MIMO in FR2, 4 × 4 in FR1
Mounting Heights	3.25 m (BS), 1.15 m (UEs A, B, C)	
2D Distances	BS-UE: 6.75 m (A), 6.35 m (B), 6.60 m (C) UE-UE: 1.80 m (A-B), 1.35 m (B-C)	

TABLE II. OVERVIEW OF MEASUREMENT DATA. AVAILABLE AT [17].

Parameter	Description/Value
Sensing Links	3, i.e., BS to UEs A, B, C
CSI Measurements	RSRP (passive metric) of mmWave and anchor cells
Time Resolution	Up to 1.5 ms using modem AT-commands
Traffic Lanes	2, each 0.6 m wide and approx. 7.0 m long Track #1 closer to UEs than Track #2
Passage Directions	Bidirectional tracks (Dir. A → C, Dir. C → A)
Road Users (L × W × H)	AGV (A): 0.55 m × 0.70 m × 1.65 m Pedestrian (P): 0.35 m × 0.50 m × 1.90 m LOS condition (L) (idle, no blockage)
Measurement Runs	420 multimodal CSI traces per UE

ering real-world CSI data of traversing users. Afterward, we explain the ML process suitable for ISAC within a factory EI deployment, facilitating factory automation and critical safety applications in Sec. III-B.

A. Design of Experiments for mmWave CSI Data Acquisition

The deployment scenario is located within a 6 m high hall featuring an evaluation area in which three commercial UEs, all at a height of 1.15 m, are served by the mmWave antenna installed at 3.2 m height in the corner of the hall. The propagation path of the LOS links is in the range of 6.65 m to 7.05 m. The new radio (NR) mmWave cell pencil beams with the synchronization signal block (SSB) identifications (IDs) 1, 2, and 3 serve UEs A, B, C. Moreover, the mmWave cell operates with a bandwidth of 800 MHz and 27.1 GHz center frequency. A sub-6 GHz long term evolution (LTE) cell provides an anchor link at 2.6 GHz with 20 dBm equivalent isotropically radiated power (EIRP) to sustain the mmWave links with both cells. Tab. I summarizes the relevant system details.

As depicted on the left side of Fig. 2, the UEs are mounted along a 7.0 m long two-lane track, each 0.6 m wide. Both AGVs and human workers, see details in Tab. II, shall traverse these lanes in either direction to move safely in the factory environment. Due to this mobility, they influence the radio channels of the UEs, connecting the machines on the factory floor.

The RAN feeds passive RSRP information along mmWave and anchor links with a time resolution of about 1.5 ms to the EI to perform the sensing task (cf. Sec. III-B). Additionally, the mmWave cell logs SSB beam IDs with 1 s time resolution. However, this allows only limited insights as more information about the UEs’ antenna array states is also needed.

We conducted systematic measurements to gather real-world mmWave data for ML model training. First, we measured each

radio link 60 times under LOS (L) conditions. After that, we captured CSI traces for AGV (A) and pedestrian (P) passing the UEs at walking speed. Specifically, we conducted 4 × 45 measurements for each vehicle type, with 45 per lane (track 1, track 2) and movement direction (Dir. A → C, Dir. C → A). Afterward, we labeled the captured CSI traces for each UE and scenario accordingly. Fig. 3 shows some traces outlining that CSI traces exhibit distinguishable characteristics depending on, e.g., road user class, passage direction, and carrier frequency. The full dataset is available under [17].

B. Direction Estimation and User Classification at the Edge

This section introduces IMMERSE’s passage direction estimation and vehicular user classification components.

1) Direction Estimation: We apply a threshold-based algorithm that detects the actual periods of user passages in the real-time CSI streams. By correlating the time offsets of detected blockages for time series acquired by UEs A, B, and C, it is possible to determine the passage direction (cf. Fig. 3). We treat this objective as a hyperparameter optimization (HPO) task to find suitable parameters for the detection algorithm. More specifically, we use the experiment execution and hyperparameter tuning library Ray Tune [18], which iteratively evaluates candidate sets of a confined search space. In this work, the search space includes the threshold sensitivity  $S_t$ , the minimum blockage length  $\tau_{min}$ , and the standard deviation  $\sigma$  for the Gaussian filter.  $S_t$  controls the detection algorithm’s susceptibility to attenuation of the radio link,  $\tau_{min}$  excludes detection owing to high-frequency fading, and  $\sigma$  controls the degree of smoothing of the raw time series data.

2) User Classification: IMMERSE leverages a multi-stage ML approach containing feature extraction and selection stages as well as iterative HPO and neural architecture search (NAS) for finding and evaluating high-performance ML and deep learning (DL) models (see middle and right columns of Fig. 2). The following paragraphs explain this in more detail.

Labeling of CSI Subsequences: The gathered CSI time series comprise 8,000 samples, where only short portions represent the actual user passages. We first manually slice these into shorter subsequences. Then, we label each subsequence

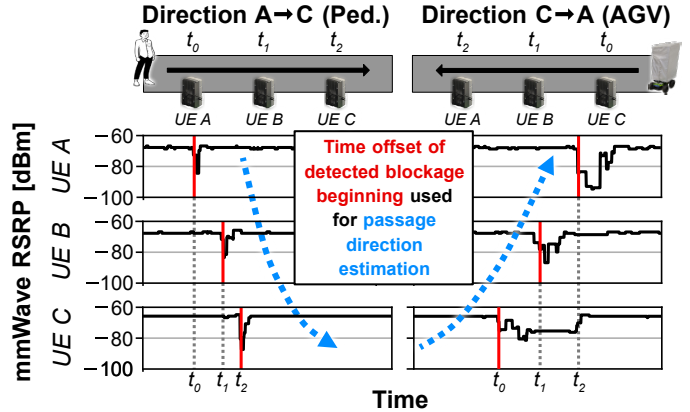


Fig. 3. Passage direction estimation is realized using detected time stamps of blockage event beginning (cf. red lines) along spatially distributed channels.

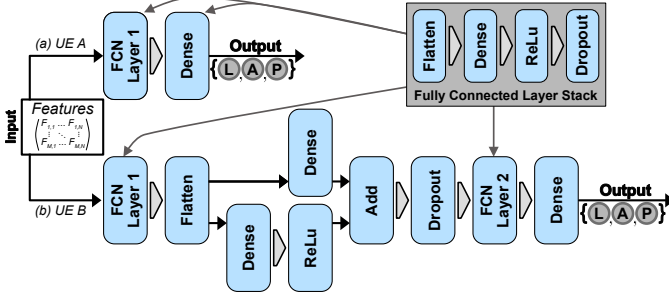


Fig. 4. Identified DNN model architectures for classifying between LOS conditions (L) and vehicle passages by AGVs (A) or pedestrians (P) traversing track 1, utilizing mmWave CSI data from (a) UE A and (b) UE B.

selecting from the set {LOS (L), AGV (A), pedestrian (P)}. We use these labeled raw CSI subsequences for convolutional neural networks (CNNs), whereas we forward them to the feature extraction step for use with deep neural networks (DNNs) and random forests (RFs).

*Feature Extraction and Selection:* We use *tsfresh* [19] to systematically deduce features, spanning domains like statistics and time series analysis (TSA), from the labeled CSI subsequences. It extracts hundreds of features that describe the characteristics of the time series. We utilize feature significance tests to reduce the feature set and thus improve the learning process. In a two-step evaluation process, hypothesis tests evaluate each candidate feature in terms of its statistical significance for the label (e. g., AGV or pedestrian), leading to vectors of  $p$ -values. Finally, the Benjamini-Yekutieli procedure selects relevant features by discarding less relevant ones. Generally, statistical tests cannot guarantee optimal feature filtering, and thus, the feature sets may vary depending on the input data. However, IMMERSE applies this statistical approach as different ML and DL models are trained and evaluated for a common feature-based input dataset.

*Hyperparameter Optimization and Neural Architecture Search:* We then pass the derived feature data to the iterative HPO and ML model evaluation process step. After defining the search space with parameters of interest and the target objective (e.g., classification accuracy), the search algorithm schedules experiment runs for different model candidates with parameter variations. The parameter search then yields the ML model performances achieved by each experiment run, allowing us to individually select suitable parameter sets for the models under investigation (MUI). IMMERSE trains and analyzes the user classification performance of CNN, DNN, and RF models in the model evaluation phase. We utilize the NAS framework [20], which runs an efficient multi-step model architecture search based on *Tensorflow* to determine the top-performing CNN and DNN models. We use the softmax cross entropy loss function for model training and define the initial learning rate within  $[10^{-6}, 10^{-2}]$ .

Fig. 4 shows the architectures of the best-performing DNN models found for mmWave data gathered by UEs A and B, classifying either (L), (A), or (P), respectively. The search algorithm creates new model candidates by stacking neural

network building blocks (e. g., dense and flatten layers) to a set of architecture candidates before randomly mutating them. Since NAS is time-consuming and computationally intensive, IMMERSE applies *Hyperband* to speed up the HPO through different means, like early stopping. IMMERSE also comprises lightweight RF model implementations provided by [21] in the classification evaluation because previous works, including our study in [13], have shown that RFs may outperform more complex DNN models on small and mid-size datasets due to their ensemble nature, fostering improved prediction performance and overfitting robustness.

#### IV. EVALUATION OF IMMERSE

This section presents and discusses IMMERSE’s performance results regarding ML-aided user classification and threshold-based passage direction estimation. First, we investigate the prediction performances for the three-type user classification task {(L), (A), (P)}, using mmWave and sub-6 GHz RSRP time series data gathered by the UEs A, B, and C, respectively. Then, we briefly discuss the feasibility of the provided multi-node system deployment regarding threshold-based user passage detection and direction estimation in Sec. IV-B.

##### A. Multi-Class User Classification

Tab. III summarizes the classification accuracy results of the best-performing models found in our extensive model search for user passages on track 1, which is close to the UEs. We use raw time series data (CNN) or extracted feature data (DNN, RF) from NR mmWave and LTE sub-6 GHz RSRP time series. We observe apparent performance gaps for the different UEs and the RAT-specific RSRP data. Regardless of the RAT, the CNN models perform significantly worse than the DNN and RF models. With the specific model architecture and input data types in mind, the CNN models try to infer the temporal relationship of each sequence step. In contrast, DNN and RF models do not need to infer such relations as we provide relevant feature data. Moreover, the labeled time series data comprises hundreds of sample values, demanding more

TABLE III. CLASSIFICATION RESULTS FOR USER PASSAGES ON TRACK 1.

CSI of UE	Sensing Metric [RSRP]	Model Accuracy [%]		
		CNN	DNN	RF
A	mmWave (27.1 GHz)	83.85	<b>100.00</b>	<b>100.00</b>
	LTE (2.6 GHz)	57.02	96.49	99.42
B	mmWave (27.1 GHz)	59.49	97.43	<b>98.78</b>
	LTE (2.6 GHz)	63.41	91.67	93.24
C	mmWave (27.1 GHz)	59.64	97.85	<b>97.09</b>
	LTE (2.6 GHz)	56.16	94.20	95.17

TABLE IV. CLASSIFICATION RESULTS FOR USER PASSAGES ON TRACK 2.

CSI of UE	Sensing Metric [RSRP]	Model Accuracy [%]		
		CNN	DNN	RF
A	mmWave (27.1 GHz)	82.86	<b>100.00</b>	<b>100.00</b>
	LTE (2.6 GHz)	67.95	97.44	<b>100.00</b>
B	mmWave (27.1 GHz)	60.16	94.67	<b>98.92</b>
	LTE (2.6 GHz)	66.67	94.78	95.44
C	mmWave (27.1 GHz)	66.94	<b>100.00</b>	<b>100.00</b>
	LTE (2.6 GHz)	63.86	90.76	91.71

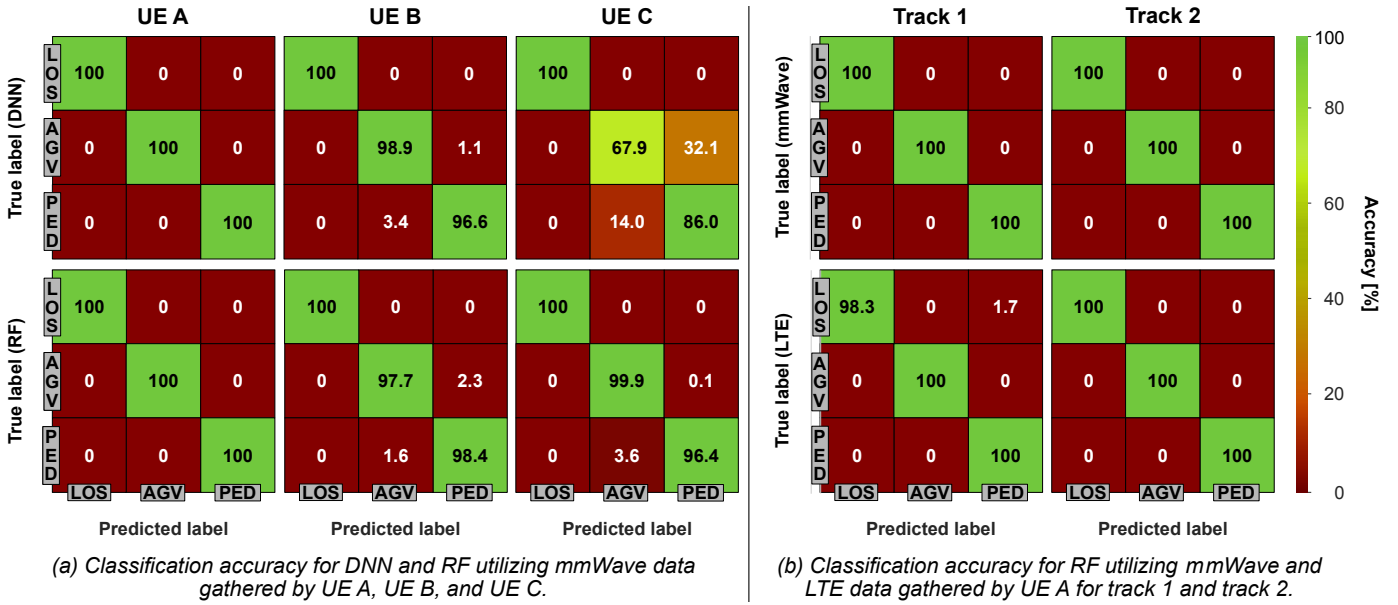


Fig. 5. Confusion matrices of the classification performances for different ML models, RAT channel data, UEs, and tracks.

intensive training and complex CNN models. Using DNN and RF with mmWave data gathered by UE A, IMMERSE achieves 100% classification accuracy, revealing its high suitability for user classification. In comparison, utilizing feature data extracted from LTE time series data of UE A leads to slightly lower accuracies, likely due to the omnidirectional LTE antennas causing more clutter within the time series. The achieved classification accuracies confirm the superiority of beam-based mmWave data, where the performance gap ranges from 1.92 to 5.76 percentage points, respectively.

Tab. IV provides the classification performances for the different UEs and RATs concerning AGV and human passages along track 2, which is more distant from the UEs. Utilizing mmWave data of UE A still allows for 100% classification accuracy. However, mmWave data from UE C also facilitates 100% accuracy using DNN and RF, increasing the score by 1.15 (DNN) and 2.91 (RF) percent points compared to the track 1 scenario. These results underline that the sensing performance improves as the distance between UEs and passing users increases.

The confusion matrices in Fig. 5 show the user-specific accuracy performances of (a) the DNN and RF models for mmWave data gathered by UEs A, B, and C and (b) the prediction performance of RF for LTE RSRP data, considering user passages on tracks 1 and 2, respectively. The UE-specific classification task (a) emphasizes the high classification accuracy when evaluating mmWave CSI data with DNN or RF. Considering mmWave data from UEs B and C leads to slightly lower performances due to the confusion of some (A) and (P) passages. This confusion is particularly significant for DNN and UE C mmWave data, where only 67.9% of (A) and 86% of (P) passages are correctly classified. This performance drop may be due to the scenario's environment, possibly resulting in cluttered time series data caused by signal reflection, etc. Regarding Fig. 5 (b), we determine classification performances

of 100% for the RF models trained with mmWave and LTE data for both user passages on tracks 1 and 2, except when using LTE data gathered in the track 1 passage scenario. The RF model falsely classifies 1.7% of (L) as (P) passages. Referring to Fig. 3, this misclassification is reasonable because short-term signal attenuation induced by pedestrians (P) can be erroneously interpreted as a deep fade.

#### B. Direction Estimation with Beamforming Analysis

In addition to the previously discussed ML-aided user type classification, we leverage the multi-node system design with spatially distributed UEs to perform threshold-based user detection and direction estimation. The confusion matrix in Fig. 6 shows the binary direction estimation performance normalized over the true conditions (Dir. C  $\rightarrow$  A, Dir. A  $\rightarrow$  C). The results reveal an almost symmetrical direction estimation performance with a mean accuracy of 97.8% and a 2.3 percentage points asymmetry. The few misclassifications result from incorrect time offset determination, which can occur if, for example, only two out of three UEs detect a passing user. However, the naive threshold-based detection and direction estimation approach achieves robust results, which is necessary to estimate a user's trajectory. In future work, the estimator can be improved using radio link-specific features.

Finally, this section considers the results of cell side beam usage. We gathered aggregated SSB beam information with an update rate of 1 s and present the relative beam activity for (L) and user passages {(A), (P)} at tracks 1 and 2, respectively. The left side of Fig. 7 shows a fair allocation of BS antenna beams with beam IDs 1 to 3, each serving one UE under LOS conditions. Considering the user passages {(A), (P)} (see right side of Fig. 7), we observe a beam switching with an unequal share of beams with IDs 1–3. In addition, previously unused beams are temporarily used, depending on whether the users traverse on track 1 (IDs 1, 4) or 2 (ID 7). This behavior

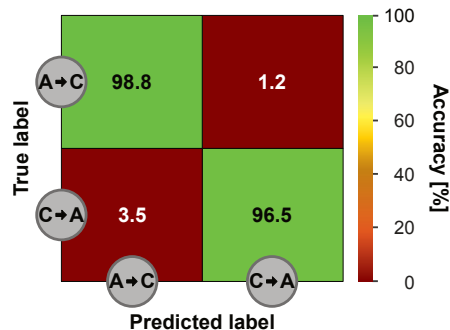


Fig. 6. Confusion matrix for passage direction estimation at the edge utilizing mmWave CSI streams from UEs *A*, *B*, and *C*.

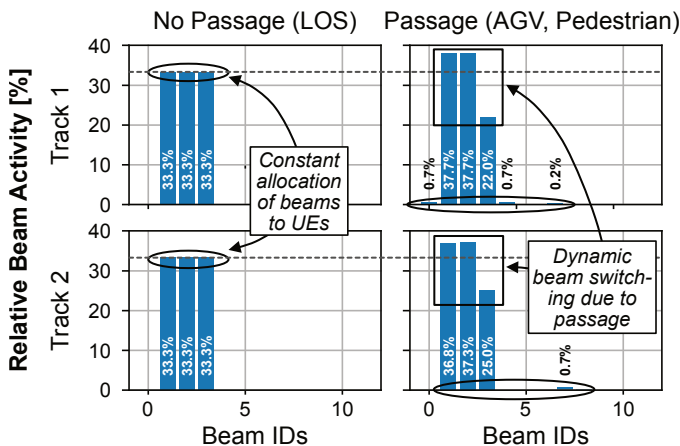


Fig. 7. Relative beam activity for multiple LOS and passage traces of pedestrians and AGVs at tracks 1 and 2.

indicates that the CSI traces are affected by the inherent beam management of the network, such that characteristic RSRP blockage behavior is only partially observed compared to traces in our recent study [13], affecting the performance of the vehicle classification and direction estimation. In future work, we would like to highlight the potential of xAPP software development, which finely tunes the beam management to optimize the sensing scheme.

## V. CONCLUSIONS

In the scope of ongoing 6G research in the field of ISAC, the exploitation of native wireless channel information enables private industry networks to cater sensing services for shop floor automation. This paper first measures cellular mmWave and anchor band channel data affected by ambient indoor mobility of AGVs and humans. We show that edge intelligence may facilitate CSI of distributed devices to detect and characterize mobility along transportation lanes.

The takeaways of this paper are as follows. Contrasting related works, we showcase RAT-external use cases of blockage detection and transfer the concept from test platforms to an actual indoor mmWave cellular system. The proposed IMMERSE approach applies current DL and lightweight ML models with gathered mmWave and sub-6 GHz channel data, highlighting their high suitability for sensing. Specifically, RF reveals a more robust classification accuracy, slightly outperforming the DNN-based method utilizing mmWave

data. Otherwise, the overall performance significantly drops using sub-6 GHz anchor band CSI data, resulting from more cluttered time series data due to omnidirectional antenna deployment. Moreover, we show that our multilink system deployment incorporating multiple UEs can estimate the moving direction of traversing users with 97.7% accuracy.

## ACKNOWLEDGMENT

This work was funded by the German Federal Ministry of Education and Research (BMBF) in the course of the 6GEM Research Hub under the grant number 16KISK038.

## REFERENCES

- [1] Nokia Bell Labs. Joint design of communication and sensing for beyond 5G and 6G systems. [Online]. Available: <https://onestore.nokia.com/asset/210300> (Accessed 2024-08-16).
- [2] S. Wu, M. Alrabeiah, C. Chakrabarti, and A. Alkhateeb, "Blockage prediction using wireless signatures: Deep learning enables real-world demonstration," *IEEE Open J. Commun. Soc.*, vol. 3, Mar. 2022.
- [3] B. Sliwa, N. Piatkowski, and C. Wietfeld, "The channel as a traffic sensor: Vehicle detection and classification based on radio fingerprinting," *IEEE IoT J.*, vol. 7, no. 8, Mar. 2020.
- [4] S. Häger, N. Gratza, and C. Wietfeld, "Characterization of 5G mmWave high-accuracy positioning services for urban road traffic," in *Proc. IEEE VTC-Spring*, Jun. 2023.
- [5] F. Liu, Y. Cui, C. Masouros, *et al.*, "Integrated sensing and communications: Toward dual-functional wireless networks for 6G and beyond," *IEEE J. Sel. Areas Commun.*, Jun. 2022.
- [6] S. Blandino, T. Ropitault, C. da Silva, *et al.*, "IEEE 802.11bf DMG sensing: Enabling high-resolution mmWave Wi-Fi sensing," *IEEE Open J. Veh. Technol.*, vol. 4, Jan. 2023.
- [7] L. Jiao, P. Wang, A. Alipour-Fanid, H. Zeng, and K. Zeng, "Enabling efficient blockage-aware handover in RIS-assisted mmWave cellular networks," *IEEE Trans. Wirel. Commun.*, vol. 21, no. 4, Apr. 2022.
- [8] A. Ali, N. Gonzalez-Prelcic, R. W. Heath, and A. Ghosh, "Leveraging sensing at the infrastructure for mmWave communication," *IEEE Commun. Mag.*, vol. 58, no. 7, Jul. 2020.
- [9] Y. Chen, J. Zhang, W. Feng, and M.-S. Alouini, "Radio sensing using 5G signals: Concepts, state of the art, and challenges," *IEEE IoT J.*, vol. 9, no. 2, Jan. 2022.
- [10] P. Susarla, M. Jokinen, N. Tervo, *et al.*, "Learning human-blockage direction prediction from indoor mmWave radio measurements," in *Proc. ICC Wkshps.*, Jun. 2023.
- [11] R. Hersyandika, Y. Miao, and S. Pollin, "Guard beam: Protecting mmWave communication through in-band early blockage prediction," in *Proc. IEEE GLOBECOM*, Dec. 2022.
- [12] A. Bonfante, L. G. Giordano, I. Macaluso, and N. Marchetti, "Performance of predictive indoor mmwave networks with dynamic blockers," *IEEE Trans. Cogn. Commun. Netw.*, vol. 8, no. 2, Jun. 2022.
- [13] M. Haferkamp, S. Häger, and C. Wietfeld, "DL-enabled road traffic monitoring services using 6G mmWave channel state information," in *Proc. 6GNet*, Oct. 2024.
- [14] M. Haferkamp, B. Sliwa, and C. Wietfeld, "A low cost modular radio tomography system for bicycle and vehicle detection and classification," in *Proc. IEEE SysCon*, Apr. 2021.
- [15] S. Häger, M. Haferkamp, and C. Wietfeld, "Beam-based 6G networked sensing architecture for scalable road traffic monitoring," in *Proc. IEEE SysCon*, Apr. 2023.
- [16] M. Danger, S. Häger, K. Heimann, S. Böcker, and C. Wietfeld, "Empowering 6G industrial indoor networks: Hands-on evaluation of IRS-enabled multi-user mmWave connectivity," in *Proc. EuCNC/6G Summit*, Jun. 2024.
- [17] M. Haferkamp. IMMERSE dataset. [Online]. Available: [https://github.com/tudo-cni/immerse\\_dataset](https://github.com/tudo-cni/immerse_dataset)
- [18] R. Law, E. Liang, R. Nishihara, *et al.*, "Tune: A research platform for distributed model selection and training," arXiv Machine Learning (cs.LG) e-prints, Jul. 2018.
- [19] M. Christ, N. Braun, J. Neuffer, and A. W. Kempa-Liehr, "Time series feature extraction on basis of scalable hypothesis tests (tsfresh – a Python package)," *J. Neurocomputing*, vol. 307, Sep. 2018.
- [20] L. Li, K. Jamieson, G. DeSalvo, *et al.*, "Hyperband: A novel bandit-based approach to hyperparameter optimization," *J. Mach. Learn. Res.*, vol. 18, no. 1, Jan. 2017.
- [21] F. Pedregosa, F. Varoquaux, A. Gramfort, *et al.*, "Scikit-learn: Machine learning in Python," *J. Mach. Learn. Res.*, vol. 12, Nov. 2011.